MODELLING AND OPTIMISATION OF A H₂-BASED ENERGY STORAGE SYSTEM IN AN AUTONOMOUS ELECTRICAL NETWORK

K.A. Kavadias[*], D. Apostolou, J.K. Kaldellis

Soft Energy Applications and Environmental Protection Laboratory
Piraeus University of Applied Sciences, P.O. Box 41046, Athens, 12201, Greece

Abstract

The European Union's 2020 climate and energy package (known as "20-20-20" targets) requests, among other key objectives, 40% of the electricity production in Greece to be supplied from Renewable Energy Sources by 2020. The main barriers for reaching this target is the intermittency of renewable energy sources combined with the penetration limits in the local electrical grids and the high seasonal demand fluctuations. In this context, the introduction of energy storage systems, comprises one of the main solutions for coping with this situation. One of the most promising technologies for storing the excess energy, that would be otherwise lost, is the production and storage of hydrogen through water electrolysis. Hydrogen can be used for supporting the electricity grid during periods of high demand but also as transportation fuel for H_2-based automobiles (e.g. fuel cell vehicles). For this purpose, a simulation algorithm has been developed, able to assess the specifications of the optimum sizing of hydrogen production storage systems. For the application of the algorithm, the area of the Aegean Sea has been selected, owed to the considerable renewable energy sources curtailments recorded in the various non-interconnected islands in the region. More specifically, the developed algorithm is applied to an autonomous electricity network of 9 islands, located at the SE area of the Aegean Sea and known as the "Kos-Kalymnos" electricity system. The results obtained designate the optimum size of the hydrogen-based configuration, aiming to maximize the recovery of otherwise curtailed renewable energy production.

1. Introduction

During the last century, the profligate exploitation of finite energy sources resulted to a negative effect on environmental, financial, and geostrategic aspects. Since the 1970s, there have been efforts to adopt a 'greener' way for covering our energy demand. Nowadays, Renewable Energy Sources (RES) based mostly on wind, solar and hydro power, are used in most developed countries, contributing significantly in the global electricity production, reaching a share of 23.7% in 2016 [1]. Particularly, in the European Union, the EU Climate Change Package, released in 2008, aims to ensure the 20–20–20 targets, meaning a 20% reduction in greenhouse gas emissions, a 20% improvement in energy efficiency, and a 20% share for renewables in the EU energy mix by the year of 2020. Specifically, the target for 2020 concerning the electricity production, includes an increase of the RES installed power share to 35% - 40% of

* Corresponding author. Tel.: +30 210 5381237 fax: +30 210 5381467.
E-mail address: kkav@puas.gr

Nomenclature

Greek Letters

a_x	Surface heat transfer coefficient, kWm^2/K
ΔH	Enthalpy of Reaction, kJ/kg
η_F	Faraday's efficiency
tga	Plateau slope of absorption

Symbols

A	Electrode's area, m2	f_1	Parameter related to Faraday's efficiency, mA^4cm^{-4}
A_{VH}	Van't Hoff parameter A	f_2	Parameter related to Faraday's efficiency
B_{VH}	Van't Hoff parameter B	f_{hys}	Hysteresis factor
C_{cw}	Thermal capacity of cooling water, J/K	f_{ps}	Plateau slope factor
C_t	Electrolyzer's overall thermal capacity, J/K	I	Electrolysis current, A
C_{tank}	MH total heat capacity, kJ/K	$k_{0,a}$	Kinetic rate coefficient, sec^{-1}
c_{H2}	Hydrogen specific heat capacity, J/kgK	$[MH]$	Number of atoms in hydride molecule
c_{H2O}	Water specific heat capacity, J/kgK	$\dot{m}_{H2}$	Mass flow rate of hydrogen, kg/s
c_{O2}	Oxygen specific heat capacity, J/kgK	$\dot{m}_{H2O}$	Mass flow rate of water, kg/s
c_p	Hydrogen specific heat at constant pressure, kJ/kgK	$\dot{m}_{O2}$	Mass flow rate of oxygen, kg/s
c_p	Hydrogen specific heat at constant volume, kJ/kgK	N_0	Initial storage level of buffer tank, mol
E_a	Activation energy, J/mol	N_{H2}	Final hydrogen stored in buffer tank, mol
E_{abs}	Absorbed Energy by the electrolyzer, kWh	$N_{H2,a}$	absorbed quantity of hydrogen in MH, mol
E_{cool}	Thermal energy removed from electrolyzer's cooling system, kWh	N_{out}	Hydrogen exiting buffer tank, mol
E_{H2loss}	Faradaic losses, kWh	n	Number of electrons to split each molecule of water
E_{loss}	Thermal energy lost to environment, kWh	$\dot{n}_{H2}$	Hydrogen production rate, mol/s
E_{sens}	Sensible heat to fluids, kWh	n_c	Number of cells in series
E_{stored}	Stored energy in the electrolyzer's mass, kWh	P_{in}	Input power of electrolyzer, kW

F	Faraday's constant, 96484.6 C/mol	P_{max}	Maximum power of electrolyzer, kW
PM_{MH}	MH molecular weight, g/mol	s_3	Anode Overvoltage Parameter 3, $V/^oC^2$
p_0	Initial pressure in buffer tank, bar	T_a	Ambient Temperature, K
p_{bf}	Pressure inside buffer tank, bar	$T_{cw,in}$	Inlet temperature of cooling water, K
p_{eq}	Equilibrium pressure, bar	$T_{cw,out}$	Outlet temperature of cooling water, K
p_{H2}	Partial pressure of hydrogen, N/m^2	T_{el}	Electrolysis temperature, K
p_{H2O}	Partial pressure of water, N/m^2	T_{H2}	Hydrogen temperature entering buffer tank, K
p_{in}	Entering hydrogen pressure in MH, bar	$T_{H2,in}$	Hydrogen temperature entering MH, K
p_{O2}	Partial pressure of oxygen, N/m^2	T_{H2O}	Temperature of entering water in electrolyzer, K
$\dot{Q}_{cool}$	Auxiliary electrolysis cooling demand, W	t_1	Cathode Overvoltage Parameter 1, m^2/A
$\dot{Q}_{gen}$	Electrolysis generated heat flux, W	t_2	Cathode Overvoltage Parameter 2, $m^2\ ^oC/A$
$\dot{Q}_{loss}$	Heat loss flux to environment, W	t_3	Cathode Overvoltage Parameter 3, $m^2\ ^oC^2/A$
Q_{MH}	MH absorption denerated heat, kJ	U_{cell}	Electrolytic cell voltage, V
$\dot{Q}_{sens}$	Heat flux with H_2, O_2, H_2O streams, W	U_{el}	Electrolysis voltage, V
$\dot{Q}_{store}$	Stored heat flux in the electrolyzer's mass, W	U_{rev}	Reversible voltage, V
R	Universal gas constant, 8.314 J/kmol	U_{rev,T,P^o}	Reversible voltage at standard conditions, V
R_t	Overall thermal resistance of electrolyzer, K/W	U_{tn}	Thermoneutral voltage, V
r_1	Empirical Ohmic Parameter 1, Ωm^2	V_{max}	Maximum volume of buffer tank, m^3
r_2	Empirical Ohmic Parameter 2, $\Omega m^2/^oC$	W_{MH}	Metal hydride mass, kg
s_1	Anode Overvoltage Parameter 1, V	X	Hydrogen to metal ratio in MH tank
s_2	Anode Overvoltage Parameter 2, $V/^oC$	z	Compressibility factor

the total electrical power installations [2].

However, the efficient exploitation of RES presents drawbacks concerning mostly their penetration in weak electrical grids. According to Kaldellis (2008) [3], wind energy

and solar energy exhibit a stochastic and variable availability respectively, enhancing the mitigation of the RES maximum penetration during the daily and seasonal electricity demand fluctuations. So, it is obvious that even in the case of high wind or solar potential, the produced energy may not be absorbed from the electrical network, resulting in a waste of energy and monetary losses for the RES investors. Furthermore, the fact that there are several remote locations (even in Europe), especially in island regions (e.g. case of the Aegean archipelago islands) where the grid is unstable and is based on high operating cost oil-fired generators, indicates the necessity of high RES systems' penetration [3].

Hence, it is essential to mitigate the intermittent nature of RES installations in order to maximize their integration both in electrical networks and in isolated off-grid consumers. Schroeder (2011) [4] suggests that there are two effective concepts to encounter with the variable outputs of RES. Demand side management by using 'smart metering' including demand response and direct load control, and energy storage by using specific arrangements in order to store excess energy whenever this is available [5]. Fig. 1 indicates the most common energy storage technologies depending on their autonomy period and power rate [6].
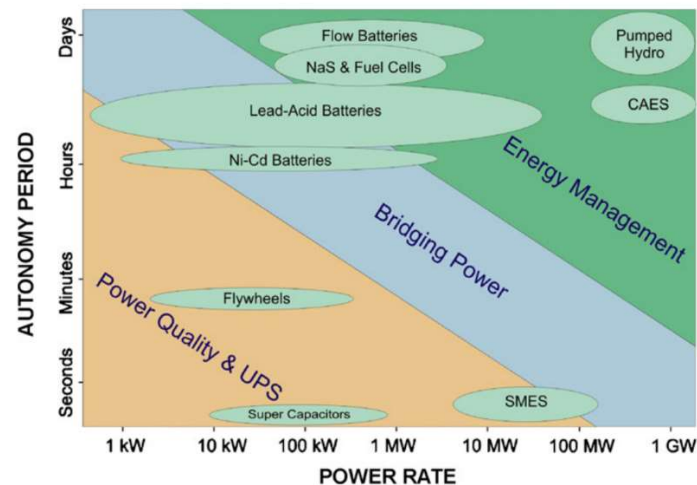

Fig. 1. Energy storage systems and their application range [6]

One of the most promising technologies for storing excess energy from RES systems during off-peak hours is the production and storage of hydrogen. Hydrogen energy storage technologies present a power rate range in the order of 10 MW and are suitable for a long term storage (see Fig. 1). Thus, H_2 can be used in almost all the applications where today fossil fuels dominate, without the harmful emissions of the last ones [7]. There are several methods for producing hydrogen from renewables with the most appropriate method for RES energy exploitation being through water electrolysis, where water splits into H_2 and O_2 through the application of direct current (DC) electricity. The most significant water electrolysis technologies include the alkaline, the proton exchange membrane (PEM) and the solid-oxide electrolysis. Large-scale alkaline electrolysis units comprise a mature technology in the industrial sector, able to produce up to 200 Nm^3/hr of hydrogen. These alkaline electrolyzers use an aqueous solution of sodium or potassium hydroxide (i.e. *NaOH, KOH*) as electrolyte, where two nickel-coated steel electrodes emerge. The two electrodes are separated via a porous membrane that only allows OH^- to pass, while hydrogen is generated at the cathode and oxygen at the anode (see Fig. 2) [8], [9].

Anode: $2OH^- (aq) \rightarrow 1/2O_2(g) + H_2O(l) + 2e^-$

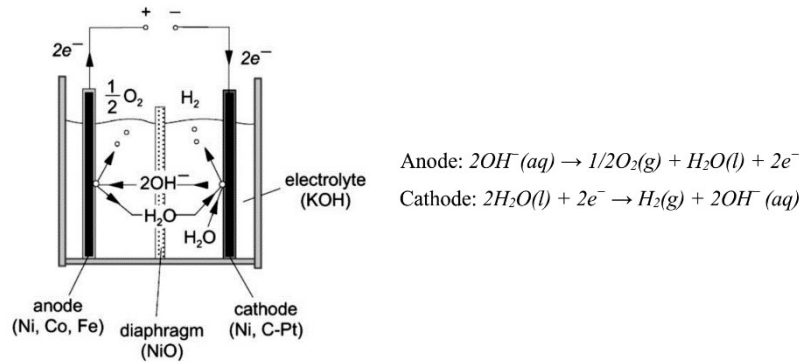Cathode: $2H_2O(l) + 2e^- \rightarrow H_2(g) + 2OH^- (aq)$

Fig. 2. Alkaline electrolysis principle [9]

On the other hand, storage of hydrogen can be accomplished with three methods: using compressed gas cylinders, special tanks, or metal hydride canisters. The first two methods, being quite land intensive, present additional disadvantages such as the high energy cost for compression and liquefaction respectively [10]. In contrast, the metal hydride storage, which is based on metal alloys' ability to reversibly absorb hydrogen at low pressure and temperature, arguably comprises the most promising technology [11].

During the last two decades, there have been efforts in modelling a combined electrolysis H_2 production-storage unit powered by RES, in order to identify all the parameters that affect such a system. Ulleberg and Molner (1997) [12] presented a *TRNSYS* simulation model for solar-hydrogen systems in order to evaluate possible system configurations at northern climates and different loads. Martin and Muradov (1999) [13] developed a model for the production and storage of hydrogen powered by a photovoltaic (PV) array. In their research they studied two cases of a system that included a PV generator, a proton exchange membrane (PEM) electrolyzer, a pressurized storage unit, a PEM fuel cell (FC), batteries and a controller. Their study was focused in the simulation of the model in order to evaluate the cooperation between the components of the energy storage system. Another research presented from Zhou and Francois (2009) [11] included the modelling and simulation of a hydrogen production system via an alkaline electrolyser and its storage in high pressure tanks while in 2010, Zini and Tartarini developed a model of a wind-hydrogen system with H_2 carbon storage [14]. More recent studies published by Khalilnejad and Riahy in 2014 and Olivier et al. in 2016 presented their simulation models for hybrid systems including RES generators coupled with hydrogen production and storage arrangements [15], [16]. Additionally in 2017, Gonzatti and Farret presented an integrated simulation of a system comprising an alkaline electrolyzer supplied from the main electric grid, metal hydride storage, and a PEM fuel cell. The results were compared with real measurement data, and revealed sufficient accuracy [17].

In this context, this paper focusses on the optimisation and proper sizing of a hydrogen based energy storage system through a simulation model. This model was based on empirical equations and depending on the input (i.e. excess power of RES), it calculates the best arrangement for producing and storing the highest amount of hydrogen.

2. Methodology

Among different energy storage technologies, hydrogen based systems present a growing interest as their potential for grid stabilization and balancing services is

evident [18]. Hence, contribution of hydrogen storage systems in weak electricity networks (such as island grids) can be considered as a solution worth examining, aiming to mainly support increased RES penetration by recovering RES curtailments.

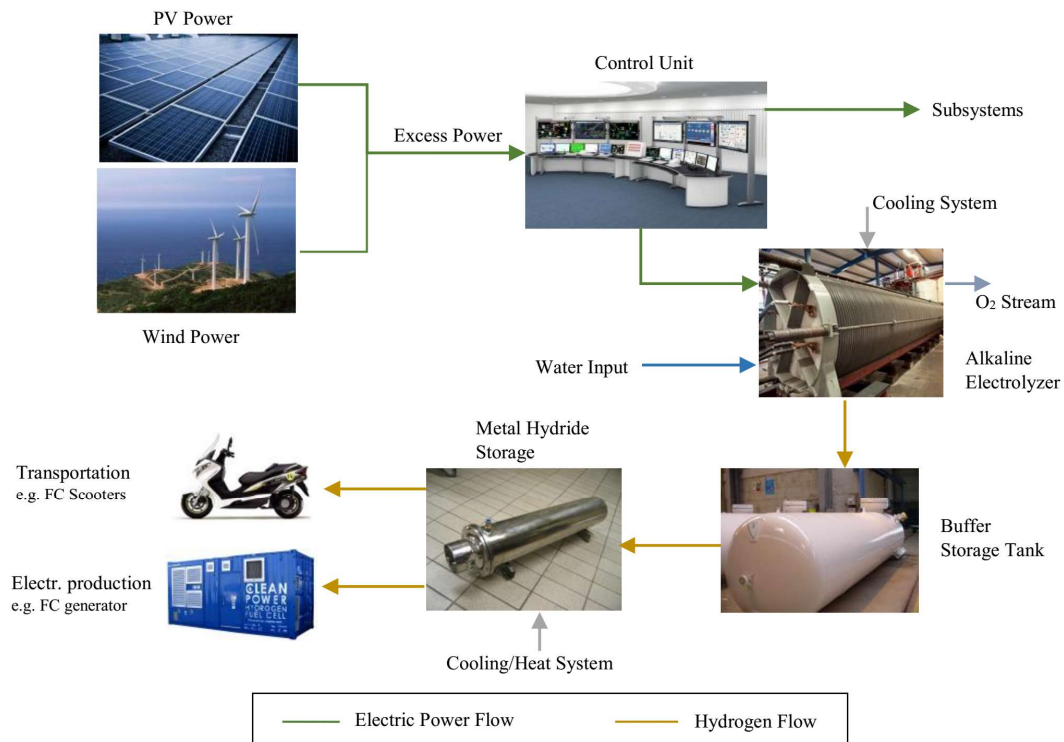Acknowledging the above, Fig. 3 presents the proposed configuration for a hydrogen production-storage system.

Fig. 3. Description of the hydrogen production-storage system

The system includes existing RES installations, along with a hydrogen system comprising of:

- An alkaline electrolyzer of maximum operational power "P_{max}" that operates at 15 bar and produces hydrogen of 99.999% purity. The electrolyzer can be supplied with RES curtailments.
- A hydrogen storage unit that includes a buffer storage tank of 200 m^3, which stores the produced hydrogen temporarily and then delivers it to the metal hydride storage system, where each of the canisters contain the alloy $MmNi_{4.5}Al_{0.5}$.
- The balance of system components such as control units, water supply, piping and auxiliary cooling systems.

The specific methodology includes the modelling of the alkaline electrolyzer for the production of hydrogen, the temporary buffer storage unit, and the metal hydride tanks for the final storage of the produced H$_2$ quantity [5]. During this research, a combination of empirical mathematical equations from multiple sources [9]–[11], [19]–[22], were used in order to obtain a more complex model that would be able to provide the best solution for storing the highest amount of the incoming excess RES energy.

Following the above, it is necessary to mention that the modelling of the system is divided into two main sections. The first section includes all the processes that take part during the hydrogen production stage and the second section concerns the

hydrogen storage procedure. It should be mentioned also that during the electrolysis process the water input of the electrolyzer (see Fig. 3) comprises of de-ionized water of low conductivity and is supposed to be always available. Additionally, the configuration does not include a storage tank for the produced O_2, which is assumed to be released to the atmosphere.

2.1 Electrolysis Model

The total reaction of water electrolysis shows that water molecules are separated under the application of electrical energy. The electromotive force (*emf*) that is necessary to split water into H_2 and O_2 is called reversible voltage (U_{rev}), which is an expression of temperature and pressure and can be calculated via the Nernst equation:

$$U_{rev} = U_{rev,T,P}^{o} - \ln\left(\frac{R \cdot T_{el}}{n \cdot F}\right) \cdot \ln\left(\frac{a_{H2O}}{a_{H2} \cdot a_{O2}^{1/2}}\right) \tag{1}$$

where, $U_{rev,T,P}^{o}$ is the reversible voltage at standard conditions in V, R is the universal gas constant in J/(mol·K), F is the Faraday constant in C/mol, n is the number of electrons to split each molecule of water, T_{el} is the operational temperature in K, and a_{H2}, a_{O2}, a_{H2O} are the activity coefficients of hydrogen, oxygen, and water accordingly. These factors are obtained by the ratio of the reactants to the atmospheric pressure.

Ulleberg (2003) [9], suggested an empirical expression that takes into account the effect of temperature on the overpotential, in order to estimate the cell voltage (U_{cell}) in V, and thereafter the electrolysis voltage:

$$U_{cell} = U_{rev} + \left(\frac{r_1 + r_2 \cdot T_{el}}{A}\right) \cdot I + \left(s_1 + s_2 \cdot T_{el} + s_3 \cdot T_{el}^2\right) \cdot \log\left[\left(\frac{t_1 + \frac{t_2}{T_{el}} + \frac{t_3}{T_{el}^2}}{A}\right) \cdot I + 1\right] \tag{2}$$

and

$$U_{el} = n_c \cdot U_{cell} \tag{3}$$

where, U_{el} is the electrolysis voltage in V, n_c is the number of the cells, I is the electrolysis current in A, A is the surface of the electrodes in m^2, r_1, r_2 are the ohmic parameters, s_1, s_2, s_3 and t_1, t_2, t_3 are the overvoltage coefficients of the anode and cathode respectively.

Hydrogen production rate ($\dot{n}_{H2}$) is highly dependent from the ion transfer between the electrodes of a cell and hence with the electrical current of the electrolysis:

$$\dot{n}_{H2} = \eta_F \cdot \left(\frac{n_c \cdot I}{n \cdot F}\right) \tag{4}$$

The Faraday's efficiency (η_F) expresses the ratio between the actual hydrogen production to the theoretical one in electrolytic processes:

$$\eta_F = \left(\frac{\left(\frac{I}{A}\right)^2}{f_1 + \left(\frac{I}{A}\right)^2} \right) \cdot f_2 \tag{5}$$

where, f_1 in mA^{4}cm^{-4}, f_2 are Faraday's parameters that depend on temperature. According to [10], these parameters can be calculated empirically as $f_1 = 2.5 \cdot T_{el} + 50$ and $f_2 = -0.00075 \cdot T_{el} + 1$.

The thermal model, that was used in this research, was proposed by Dieguez et al. (2008) [19] and was based on the model developed by Ulleberg (2003) [9]. The thermal energy balance equals to:

$$C_t \cdot \frac{dT}{dt} = \dot{Q}_{gen} - \dot{Q}_{loss} - \dot{Q}_{cool} - \dot{Q}_{sens} \tag{6}$$

with,

$$\dot{Q}_{gen} = I \cdot n_c \cdot \left(U_{cell} - U_{tn} \right) \tag{7}$$

$$\dot{Q}_{loss} = \frac{1}{R_t} \cdot \left(T_{el} - T_a \right) \tag{8}$$

$$\dot{Q}_{sens} = \left(\dot{m}_{H2} \cdot c_{H2} \right) \cdot \left(T_{el} - T_a \right) + \left(\dot{m}_{O2} \cdot c_{O2} \right) \cdot \left(T_{el} - T_a \right) + \left(\dot{m}_{H2O} \cdot c_{H2O} \right) \cdot \left(T_{el} - T_{H2Oi} \right) \tag{9}$$

$$\dot{Q}_{cool} = C_{cw} \cdot \left(T_{cw,\, in} - T_{cw,\, out} \right) \tag{10}$$

where, C_t is the overall thermal capacity of the electrolyzer in J/°C, Q_{gen} is the generated heat in W, Q_{loss} is the heat loss transfer to the environment in W, Q_{cool} is the heat removed from the apparatus via the cooling system in W, Q_{sens} includes the enthalpy leaving the system with the H_2 and O_2 produced streams along with the heat transferred from the device to the incoming deionized water in W, R_t is the overall thermal resistance of the electrolyzer in K/W, T_a is the ambient temperature in K, m_{H2}, m_{O2}, and m_{H2O} are the mass flow rates in kg/sec of the hydrogen, oxygen and inlet water respectively, c_{H2}, c_{O2}, c_w are the specific thermal capacities in J/(kg·K) of the hydrogen, oxygen and inlet water, T_{H2Oi} is the temperature of the entering water in K, C_{cw} is the thermal capacity of the cooling water in J/K, $T_{cw,in}$ is the inlet temperature of cooling water, and $T_{cw,out}$ is the outlet temperature of the cooling water in K.

U_{tn} is the thermoneutral voltage which depends on the operational temperature of the electrolyzer (in °C) and expressed as [23]:

$$U_{tn} = 1.4850 - (1.49 \cdot 10^{-4} \cdot T_{el}) - (9.84 \cdot 10^{-8} \cdot T_{el}{}^2) \tag{11}$$

2.2 Buffer Storage Model

The produced hydrogen from the water electrolysis process is initially stored in a buffer tank. During the simulation, the quantity of H_2 that is stored in the vessel (N_{H2}) can be calculated as:

$$N_{H2} = N_0 + n_{H2} - N_{out} \tag{12}$$

where, N_{H2} is the final hydrogen stored quantity in mol, N_0 is the initial storage level in mol and N_{out} is the quantity of hydrogen that exits the tank in mol.

The pressure (p_{bf}) inside the buffer storage tank can be estimated through the equation proposed by Gorgun [24]:

$$p_{bf} = p_0 + \frac{z \cdot (N_{H2} \cdot R \cdot T_{H2})}{PM_{H2} \cdot V_{max}} \tag{13}$$

where, p_0 is the initial pressure in the tank, z is the compressibility factor that is equal to 1 if pressure is below 2000 psi, T_{H2} is the temperature of the entering hydrogen in the buffer tank in K (approximately equal to the operational temperature of the electrolyzer (T_{el})), PM_{H2} is the molar mass of hydrogen, and V_{max} is the maximum volume of the storage vessel in m³.

2.3 Metal Hydride Storage Model

During the last decades, research on tanks, containing metal alloys in a powder form that have the capability to reversibly absorb hydrogen, has given significant results. These metal hydride tanks present several benefits compared to the other storage devices because they can store large quantities of hydrogen at generally low pressure and temperature. However, their large weight comprises a drawback, especially for portable applications.

Metal hydride storage devices are usually cylindrical and include the steel shell, the metal alloy material, the thermal fluid channels for regulation of the temperature, the channel where the hydrogen flows, and several auxiliary components that are necessary for a proper storage process [22].

The concept of equilibrium pressure in metal hydride storage is significant because it determines the absorption-desorption processes. If the pressure of the incoming hydrogen gas is above the equilibrium, hydrogen is absorbed. Equilibrium pressure depends on the temperature and can be calculated via the Van't Hoff equation [21]:

$$p_{eq} = \exp\left(\frac{A_{VH}}{T_{MH}} + B_{VH} + f_{ps} + f_{hys} \right) \tag{14}$$

where, p_{eq} is the equilibrium pressure in bar, A_{VH}, B_{VH} are Van't Hoff constants, T_{MH} is the temperature of the metal hydride in K, f_{hys} is the hysteresis factor which is related to the material used, and f_{ps} is the plateau slope factor equal to $f_{ps} = (X - X_\infty) \cdot tga$, where X is the hydrogen to metal ratio (i.e. hydrogen concentration), X_∞ is the maximum hydrogen concentration, and tga is the slope of the plateau (a constant related to the material used).

Based on Gambini et al. [22], the hydrogen concentration rate in the metal hydride tank during absorption can be estimated as:

$$\frac{dX}{dt} = k_{0,a} \cdot \exp\left(\frac{-E_a}{R \cdot T_{MH}} \right) \cdot \ln\left(\frac{p_{in}}{p_{eq}} \right) \cdot (X_\infty - X) \tag{15}$$

where, dX/dt is the variation in hydrogen concentration, $k_{0,a}$ is the kinetic rate coefficient during absorption in sec⁻¹, E_a is the activation energy of absorption in J/mol, R is the universal gas constant in J/(mol·K), and p_{in} is the pressure of the entering hydrogen in bar, which equals to the pressure inside the buffer tank (p_{bf}) .

Subsequently, the quantity of the stored hydrogen in the metal hydride tank equals to:

$$N_{H2,a} = X \cdot \frac{[MH] \cdot W_{MH}}{2 \cdot PM_{MH}}$$ (16)

where, $N_{H2,a}$ is the absorbed quantity of hydrogen in mol, MH is the number of atoms in the hydride molecule, W_{MH} is the mass of the metal hydride tank in kg, and PM_{MH} is the molecular weight of the metal hydride in kg/mol.

Based on equations (15) and (16), it is obvious that the concentration and therefore the absorbed quantity of hydrogen are influenced by the hydride's temperature. So, Gambini (1994) [21] proposed an analytical model which correlates the mass and heat transfer processes during the absorption of hydrogen in the metal hydride tank:

$$C_{\text{tank}} \frac{dT}{dt} = \left[a_x \frac{dX}{dt} \cdot (\Delta H + c_p \cdot T_{H2,in} - c_v \cdot T_{MH}) \right] - \frac{dQ}{dt}$$ (17)

with:

$$a_x = \frac{[MH] \cdot W_{MH} \cdot PM_{H2}}{2 PM_{MH}}$$ (18)

where, C_{tank} is the total heat capacity of the system in kJ/K, α_x is a coefficient which relates the hydrogen concentration and the hydrogen flow rate in kg, ΔH is the reaction's enthalpy in kJ/kg, c_p, c_v are the specific heat of hydrogen in constant pressure-volume in kJ/(kg·K) respectively, $T_{H2,in}$ is the temperature of the incoming hydrogen in K, T_{MH} is the temperature of metal hydride in K, Q is the generated heat in kJ, MH is the number of atoms in the hydride molecule, W_{MH} is the mass of the metal hydride tank in kg, PM_{MH} is the molecular weight of the metal hydride in gr/mol, and PM_{H2} is the molecular weight of the hydrogen in gr/mol.

2.4 Model Development

In order to minimise the requested input parameters, the model was based on a typical alkaline electrolyzer operating at 15 bar pressure, where electrolytic cells are connected in series (i.e. bipolar design) for avoiding high current values. In this way, by adding cells, maximum power increases due to voltage increase. Fig. 4 indicates the cell voltage and current curves at different operational temperatures of a typical electrolyzer estimated from the model application.
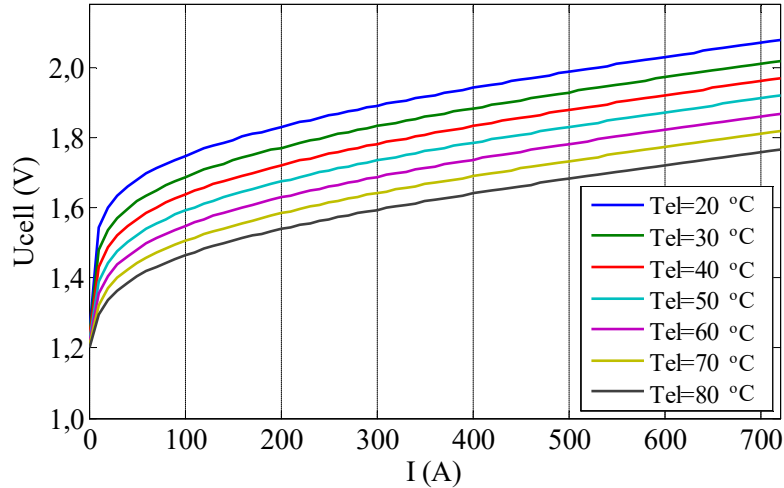
Fig. 4. Electrolysis cell voltage-current curves

On the other hand, the hydrogen absorption capability of the specific metal hydride tank ($MmNi_{4.5}Al_{0.5}$), which equals to around 320 mol/640 gr of H_2, has been estimated by the model and is depicted in Fig. 5a. Fig. 5b indicates the heat produced during the hydrogen absorption. In addition, based on Figure 5, at 230 sec 319 mol of hydrogen have been absorbed (99% of total absorption) and the thermal energy generation approaches to 0.
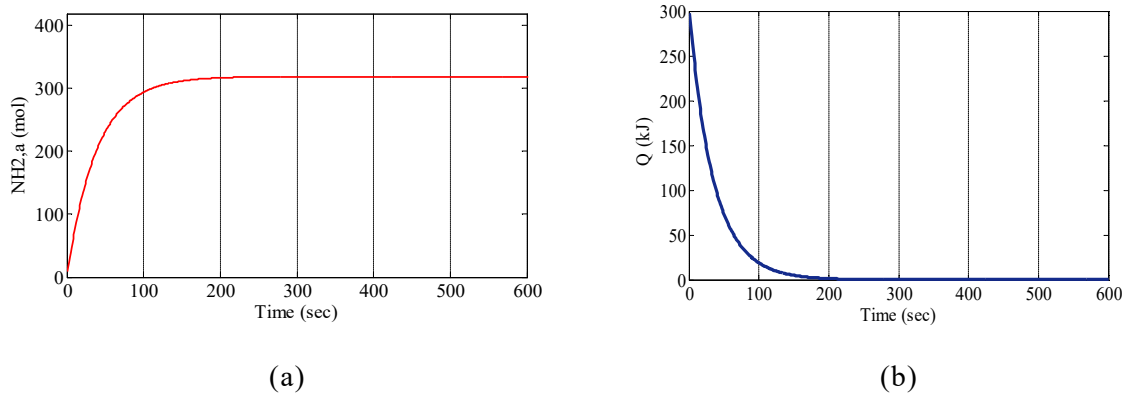

(a)

(b)

Fig. 5. Absorption capability of the metal hydride tank (a) and heat produced during H_2 absorption (b)

In order to designate the optimum size of the electrolyzer and therefore the system's additional parameters (e.g. hydrogen production, efficiency), an integrated algorithm was developed based on a set of equations describing the electrolysis and the hydrogen buffer storage processes (see Eq. 1 to 13). The model calculates the maximum hydrogen production that can be achieved for a given range of electrolyzers. The capacity of the investigated electrolyzers is based on the cell voltage-current curves (see Fig. 4), the available power input and the operational temperature, which determine the required number of electrolytic cells. The storage procedure was developed also through the empirical equations 14 to 17, which describe the mass transfer of hydrogen inside the metal hydride tanks, and the thermal phenomena that occur during the absorption of hydrogen.

The flowchart in Fig. 6 presents the algorithm used for the calculation of the electrolysis-storage parameters.
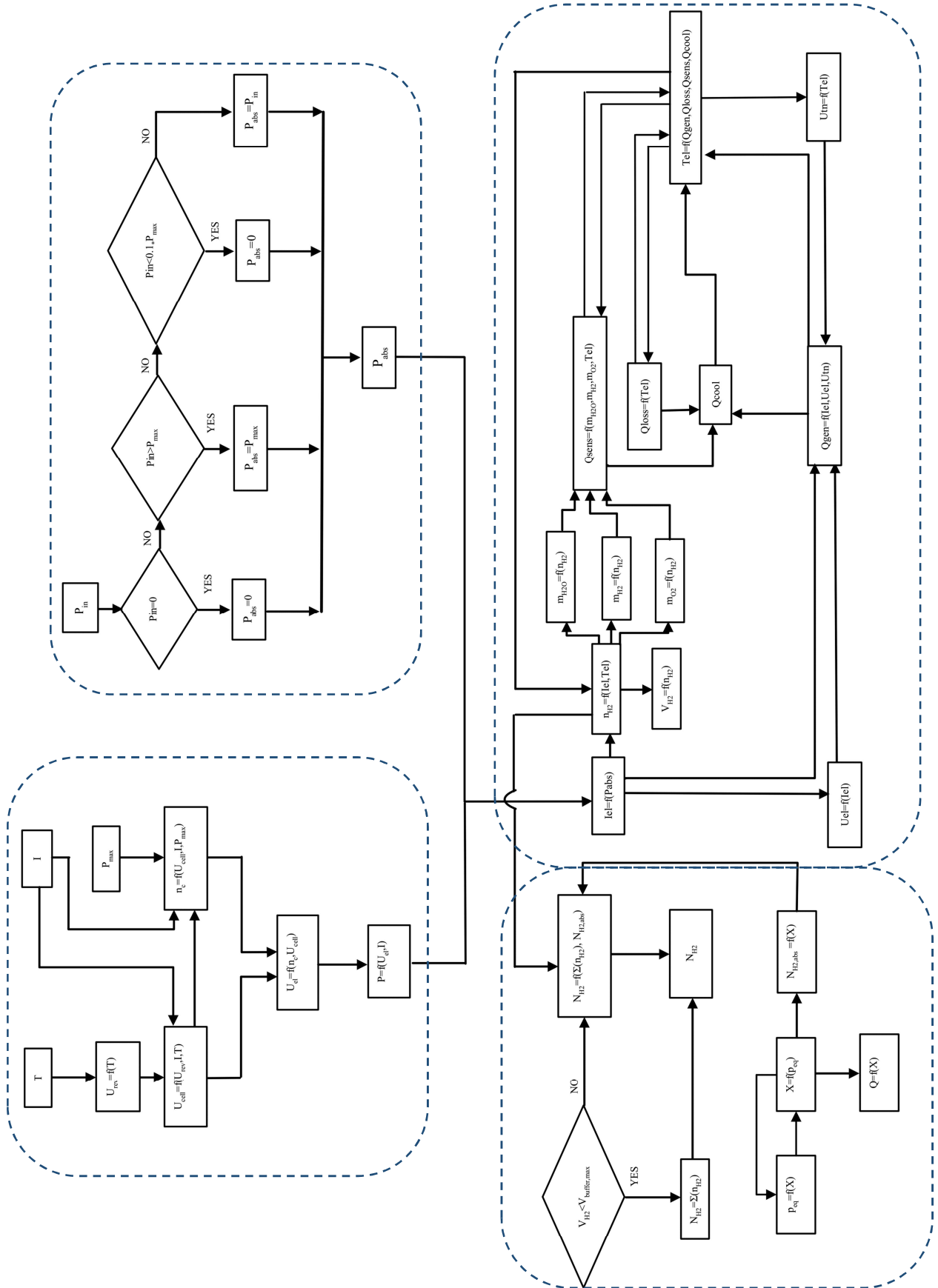
Fig. 6. Electrolysis-Storage developed algorithm

The upper left section concerns the absorbed power by different electrolyzers depending on the latter operational power range (e.g. 10% to 100%) and the respective available input. The lower left part of the block diagram explains the estimation of the current-power equations at different operational temperatures, between 20°C and 80°C, for different values of current ranging from 0 A to 720 A. The electrolysis simulation is schematically presented at the upper right part and finally the storage procedure is depicted at the lower right section.

In this regard, the algorithm estimates in a loop mode the appropriate size of the electrolyzer for storing the maximum available excess RES energy, and calculates the parameters associated with the H_2 production-storage procedure (e.g. hydrogen production, efficiency of electrolysis, etc).

3. Case Study

In order to examine the validity of the developed algorithm concerning the storage of the rejected energy coming from RES installations, an autonomous electrical network such as the one of an island has been used as a case study. Nowadays, the contribution of RES production in the non-interconnected islands of Greece reaches 21.8% [25], which is indicative of the quality of the local RES resources and also of the potential to support the accomplishment of the 40% RES target by 2020, this time at the national level [26]. To this end, the Kos-Kalymnos autonomous grid (see Fig. 7), comprising of 9 islands covers a big part of the Dodecanese complex, featuring excellent wind and solar potential and thus suggesting an area of major interest for harvesting RES resources. Despite the high-quality RES potential of the area however, the Kos-Kalymnos system is currently based on thermal power generation, with its average contribution per annum being in the order of 84% [27]. The conventional power stations comprise two oil-based plants of around 120 MW, one in Kos (102 MW) and one in Kalymnos (18 MW). On the other hand, installed RES capacity includes mainly wind and PV power installations. Wind and PV power capacity reaches 15.2 MW and 8.78 MW respectively [25].
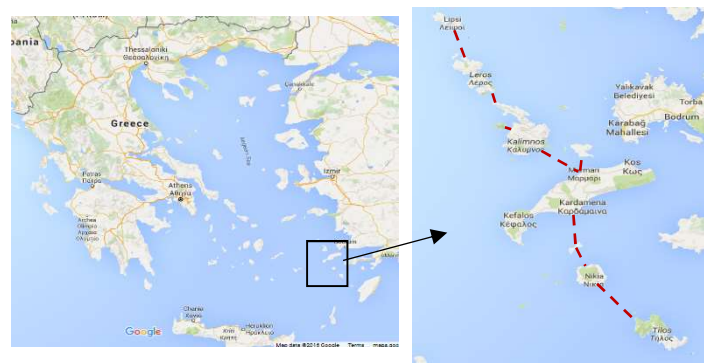

Fig. 7. The "Kos-Kalymnos" system interconnection (9-island complex)

In this context, Fig. 8 presents the daily electricity generation and annual share in the "Kos-Kalymnos" system for 2013, where it is obvious that the RES contribution in the local generation mix is much lower than the respective of the conventional thermal power plants which reached 87%. To this end, it is necessary to mention that local RES stations must comply with the minimum residual load deriving from the dynamic penetration limit set by the local operator (i.e. 30% over the instantaneous load demand) on the one hand, and from the technical minima of local thermal power stations (TPS) on the other [28].

As it is obvious from Fig. 9a, most of the electricity produced from the existing RES stations has been absorbed from the network contributing to the increased electricity demand during the summer months (see Fig. 8). However, RES curtailments during the year are still frequent and discourage the implementation of new RES projects (see Fig. 9b).
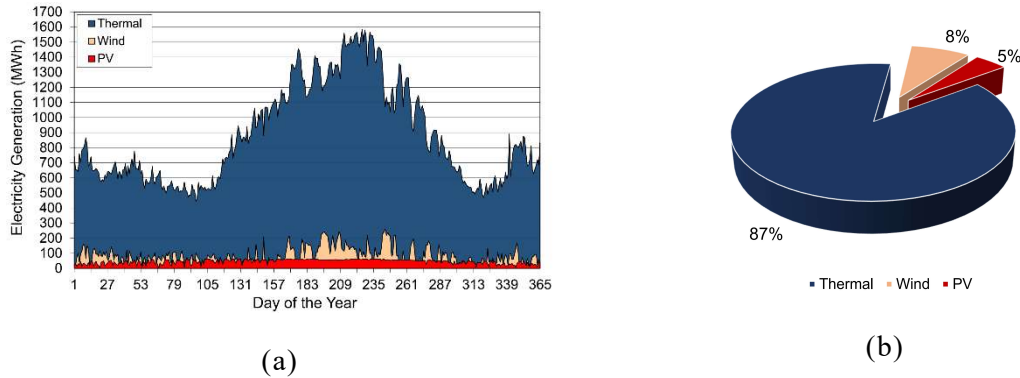

(a)

(b)

Fig. 8. Electricity generation in "Kos-Kalymnos (a) and Electricity generation share in "Kos-Kalymnos" (b) during 2013

At the same time, it is important to note that the use of imported oil for the operation of the TPSs results to increased electricity production cost and local air pollution phenomena [3], [29].
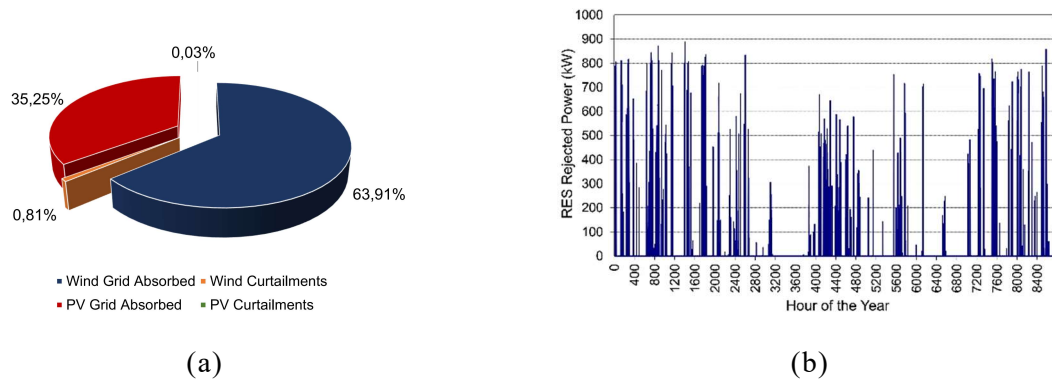

(a)

(b)

Fig. 9. RES electricity generation share in "Kos-Kalymnos" (a) and RES curtailments in "Kos-Kalymnos" (b) during 2013

According to the non-interconnected management of the Public Power Corporation S.A. of Greece, in 2014 the "Kos-Kalymnos" TPSs' demand for fuel reached 65,649 tn of mazut and 409 tn of diesel oil. The cost of the imported fuels rose to 35.6 M€, while the total cost of the produced electricity reached 47.6 M€ [30]. Hence, one can figure out that fuel imports comprise 75% of the total expenditures of the TPSs operation. The average cost of electricity generation for 2014 can be calculated to 153 €/MWh which is significant compared to the average cost of production in the mainland (2014) which did not exceed 58 €/MWh [31].

4. Results and Discussion

4.1 Simulation of the H_2 System

In order to calculate the characteristics of the optimum hydrogen production-storage configuration able to absorb the maximum available excess RES rejected energy in

the "Kos-Kalymnos" system which equals to around 398 MWh, a *MATLAB* code was developed based on the model described in the previous sections. As an input to the model, the rejected power profile (curtailments), presented in Fig. 9b, was introduced. The sizing of the hydrogen production system has been estimated through the examination of 195 electrolyzers with a range of rated power between 100 kW and 4 MW. To this end, Fig. 10 illustrates the percentage of the stored energy estimated for these electrolyzers through the model.

According to Fig. 10 for absorbing the maximum rejected RES energy (i.e. around 71%), an electrolyzer of 1.26 MW capacity is necessary. It should be noticed that although the maximum RES rejected power reaches 900 kW (see Fig. 9(b)), the capacity of the optimum electrolyzer is much higher due to its operational power limits, which range between 10% and 100% of its nominal capacity.
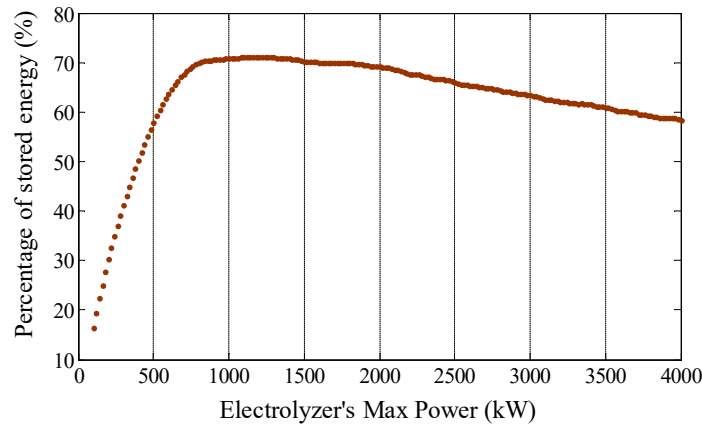

Fig. 10. Percentage of stored energy at different values of electrolyzer's capacity

Subsequently, the specific electrolyzer of 1.26 MW rated power has been used by the model to calculate the parameters (e.g. H_2 production) during its annual operation based on the time series data of RES curtailments in the examined autonomous electrical network.

In Fig. 11, the produced hydrogen mass rate on an annual basis is depicted. According to Fig. 11 the daily quantity of the produced hydrogen reaches 288 kg, while the average daily value is approximately 20 kg.
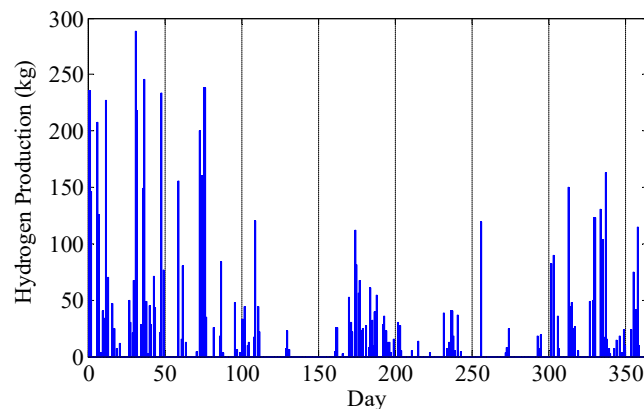

Fig. 11. Hydrogen production rate

The energy balance during the operation of the electrolyzer can be seen in Fig. 12. The 73% of the absorbed energy (E_{abs}) is stored as hydrogen (H_2). The rest 22%

represents the generated heat during the operation of the system, which is further divided in the thermal energy removed via the auxiliary cooling (E_{cool}) system, the thermal energy lost to the environment (E_{loss}), the thermal energy stored in the mass of the electrolyzer (E_{stored}), the sensible heat leaving the system with the hydrogen-oxygen streams and the thermal energy transferred to the incoming water (E_{sens}). Finally, E_{H2loss} represents the last 5% of the absorbed power and expresses the faradaic losses occurring during the operation of the device.
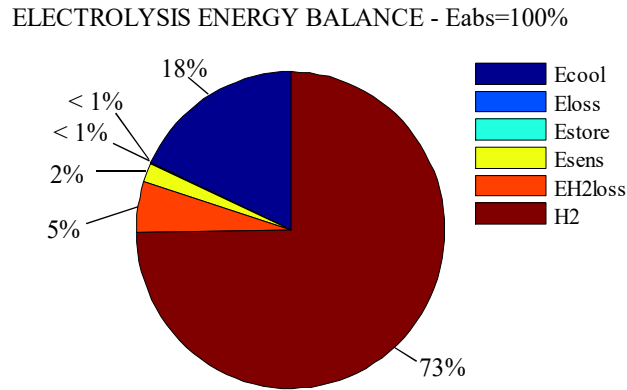
ELECTROLYSIS ENERGY BALANCE - Eabs=100%

Fig. 12. Electrolysis energy balance

The produced hydrogen via the electrolysis process is stored in the 200 m^3 buffer storage tank prior to its storage in the metal hydrides. Fig. 13 illustrates the variation of the hydrogen concentration inside the buffer storage tank. It is obvious that in periods of zero H$_2$ production, the hydrogen quantity inside the tank is used for filling the metal hydride canisters until its full depletion. Fig. 14a indicates the equilibrium pressure variation during the absorption of hydrogen along with the relationship between the equilibrium pressure and the absorbed hydrogen in the metal hydride canister (Fig. 14b). Equilibrium pressure at the beginning equals to around 3.85 bar. As concentration of hydrogen increases the canister's temperature rise, resulting to an increase of the equilibrium pressure to 4.2 bar and suggesting a reduced rate of absorption (Fig. 13). A summary of the results of the H$_2$ production-storage simulation is given in Table I.
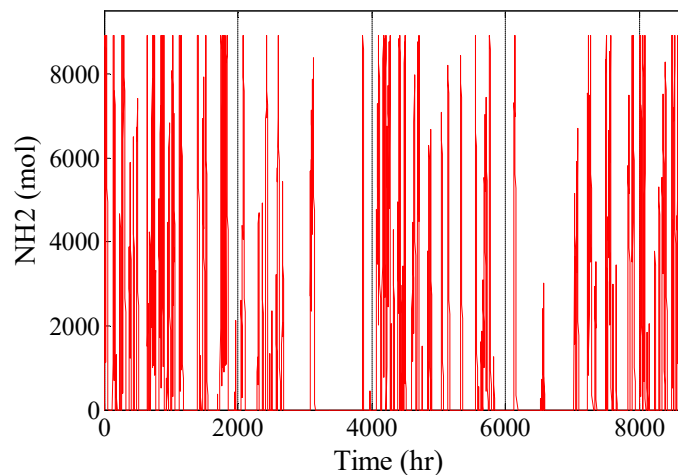

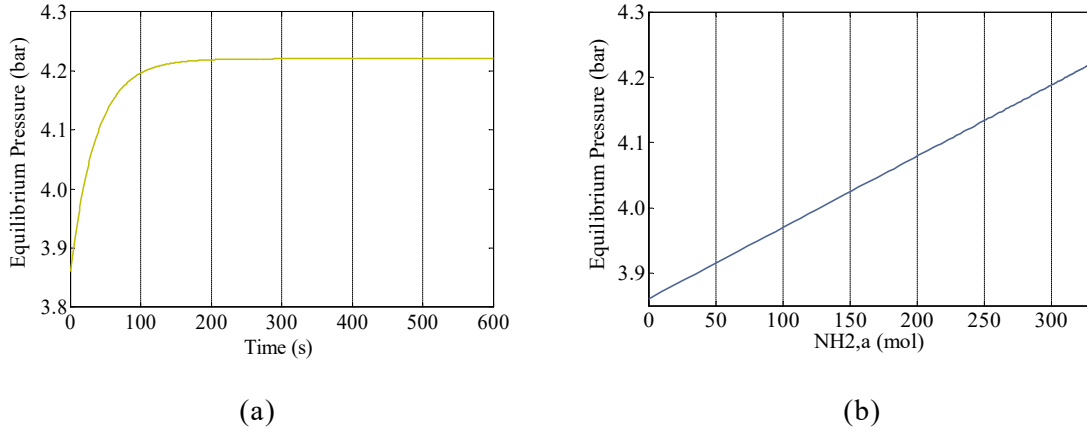Fig. 13. Hydrogen concentration in buffer tank

Fig. 14. Equilibrium pressure during hygrogen storage in one metal hydride tank(a) and equilibrium pressure dependancy with H_2 concentration (b)

Table I: Simulation application results for the "Kos-Kalymnos" electric network

Annual Operation of the Hydrogen Production – Storage System		
Parameter	Value	Units
Maximum Operational Power	1.26	MW
Minimum Operational Power	126	kW
RES Rejected Energy	398	MWh
Total Absorbed Energy	385	MWh
Annual Hydrogen production	7226	kg
Total Storage Capacity of Metal Hydride Canisters	3.58×10^6	mol
Average Electrolysis Electrochemical Efficiency	72.9%	-
Average Electrolysis Overall Efficiency	62.9%	-
Average Storage Efficiency	89.7%	-
Average Total Efficiency (production-storage)	56.4%	-

Based on the high heating value of hydrogen (HHV), the average efficiency for producing hydrogen equals to 63%. The difference between this value and the electrolysis electrochemical efficiency arises due to the energy needed for the cooling processes of the electrolyzer. Additionally, by assuming that there is no hydrogen loss through the piping system, the storage efficiency equals to around 89.7% due to the auxiliary cooling system of the metal hydride canisters. In this context, the average total efficiency of the system drops to 56%.

4.2 Produced Hydrogen Utilisation

In order to comprehend the significance of maximising the recovery of the otherwise curtailed RES energy, it would be beneficial to examine the advantages of using the produced hydrogen for supporting the "Kos-Kalymnos" electrical network or for transportation purposes (e.g. fuel call scooters).

The annual production of hydrogen has been calculated via the model to 7226 kg. Based on the HHV of H_2 (i.e. 33.4 kWh/kg), the energy of this quantity equals to around 241.3 MWh (or 63% of total absorbed energy). One of the most promising

applications for producing electricity via hydrogen is the use of fuel cells. Nowadays, according to the US Department of Energy [32], a fuel cell system is able to produce electricity with electrical efficiencies between 50% and 60%. In this context, and by assuming that BOP efficiency is around 90%, the available energy for supporting the "Kos-Kalymnos" electrical network can be estimated to approximately 120 MWh. Hence, a significant amount (i.e. above 30%) of the rejected RES energy that otherwise would be lost, may be returned to the grid during periods of high demand.

On the other hand, the quantity of the produced H_2 can also be used as transportation fuel. According to Tso et al. (2012) [33], the average consumption of a light FC scooter with an output of around 1 kW equals to around 1.9 g/km. By taking into account that the longest traveling route of the islands' complex is 40 km, the necessary daily hydrogen fuel for one scooter would be 76 g or 0.076kg. Based on this value and the estimated average daily production of hydrogen, an indicative number of FC scooters that can be used on a daily basis reaching approximately 263 (with total daily covered distance of 10520 km).

5. Conclusions

An integrated algorithm has been developed in *MATLAB* software platform in order to estimate the optimum solution of a hydrogen based energy storage system in terms of maximum recovery of RES curtailments. The algorithm can be applied to different cases of power input time series and provide significant results for the optimum sizing of a H_2-based energy storage system. According to the results obtained from the "Kos-Kalymnos" autonomous network case study a considerable amount of hydrogen can be generated from the curtailments of RES power plants located in the specific region, with an average efficiency higher than 62%, while the overall average efficiency of the production-storage processes has been estimated to 56.4%.

In this respect, RES energy can be recovered via hydrogen generation and used either to support the grid (with the employment also of fuel cells) by returning a significant share of the rejected energy (i.e. 30%) or for transportation purposes with a substantial cost benefit for the local communities. The daily operation of 263 fuel cell scooters is able to reduce the petrol consumption in the islands' complex for transportation purposes and promote "green" mobility.

On the other hand, new RES investments would become more cost-efficient due to the minimisation of curtailments, while new business opportunities would arise in the sectors of hydrogen backup power and mobility. To this end, further research is needed to also take into account financial aspects of the problem investigated, evaluating the economic viability of such a hydrogen storage system.

REFERENCES

[1] REN21, 'Renewables 2016 Global Status Report', Paris, 2016.

[2] A. Jaeger-Waldau *et al.*, *Renewable Energy Snapshots 2012.* Luxembourg: Publications Office, 2013.

[3] J. K. Kaldellis, 'Integrated electrification solution for autonomous electrical networks on the basis of RES and energy storage configurations', *Energy Convers. Manag.*, vol. 49, no. 12, pp. 3708–3720, Dec. 2008.

[4] A. Schroeder, 'Modeling storage and demand management in power distribution grids', *Appl. Energy*, vol. 88, no. 12, pp. 4700–4712, Dec. 2011.

[5] D. Apostolou, 'Analytical Simulation of a Combined Electrolysis for Hydrogen Production – H2 Storage', Heriot Watt, Edinburgh, UK, 2015.

[6] J. K. Kaldellis, D. Zafirakis, and K. Kavadias, 'Techno-economic comparison of energy storage systems for island autonomous electrical networks', *Renew. Sustain. Energy Rev.*, vol. 13, no. 2, pp. 378–392, Feb. 2009.

[7] F. Barbir, 'PEM electrolysis for production of hydrogen from renewable energy sources', *Sol. Energy*, vol. 78, no. 5, pp. 661–669, May 2005.

[8] P. Millet and S. Grigoriev, 'Chapter 2 - Water Electrolysis Technologies A2 - Gandía, Luis M.', in *Renewable Hydrogen Technologies*, G. Arzamendi and P. M. Diéguez, Eds. Amsterdam: Elsevier, 2013, pp. 19–41.

[9] Ø. Ulleberg, 'Modeling of advanced alkaline electrolyzers: a system simulation approach', *Int. J. Hydrog. Energy*, vol. 28, no. 1, pp. 21–33, Jan. 2003.

[10] M. J. Khan and M. T. Iqbal, 'Analysis of a small wind-hydrogen stand-alone hybrid energy system', *Appl. Energy*, vol. 86, no. 11, pp. 2429–2442, Nov. 2009.

[11] T. Zhou and B. Francois, 'Modeling and control design of hydrogen production process for an active hydrogen/wind hybrid power system', *Int. J. Hydrog. Energy*, vol. 34, no. 1, pp. 21–30, Jan. 2009.

[12] Ø. Ulleberg and S. O. Mørner, 'TRNSYS simulation models for solar-hydrogen systems', *Sol. Energy*, vol. 59, no. 4, pp. 271–279, Apr. 1997.

[13] E. Martin and N. Muradov, 'MODELING OF SUSTAINABLE HYDROGEN PRODUCTION/STORAGE ENERGY SYSTEMS FOR REMOTE APPLICATIONS', presented at the Fuel Chemistry Division Symposia, New Orleans, USA, 1999.

[14] G. Zini and P. Tartarini, 'Wind-hydrogen energy stand-alone system with carbon storage: Modeling and simulation', *Renew. Energy*, vol. 35, no. 11, pp. 2461–2467, Nov. 2010.

[15] A. Khalilnejad and G. H. Riahy, 'A hybrid wind-PV system performance investigation for the purpose of maximum hydrogen production and storage using advanced alkaline electrolyzer', *Energy Convers. Manag.*, vol. 80, pp. 398–406, Apr. 2014.

[16] P. Olivier, C. Bourasseau, and B. Bouamama, 'Modelling, simulation and analysis of a PEM electrolysis system', *IFAC-Pap.*, vol. 49, no. 12, pp. 1014–1019, 2016.

[17] F. Gonzatti and F. A. Farret, 'Mathematical and experimental basis to model energy storage systems composed of electrolyzer, metal hydrides and fuel cells', *Energy Convers. Manag.*, vol. 132, pp. 241–250, Jan. 2017.

[18] K. Harrison and M. Peters, 'Renewable Electrolysis Integrated System Development & Testing', presented at the 2014 DOE Hydrogen and Fuel Cells Program Review, 2014.

[19] P. M. Diéguez, A. Ursúa, P. Sanchis, C. Sopena, E. Guelbenzu, and L. M. Gandía, 'Thermal performance of a commercial alkaline water electrolyzer: Experimental study and mathematical modeling', *Int. J. Hydrog. Energy*, vol. 33, no. 24, pp. 7338–7354, Dec. 2008.

[20] M. Carmo, D. L. Fritz, J. Mergel, and D. Stolten, 'A comprehensive review on PEM water electrolysis', *Int. J. Hydrog. Energy*, vol. 38, no. 12, pp. 4901–4934, Apr. 2013.

[21] M. Gambini, 'Metal hydride energy systems performance evaluation. Part A: Dynamic analysis model of heat and mass transfer', *Int. J. Hydrog. Energy*, vol. 19, no. 1, pp. 67–80, Jan. 1994.

[22] M. Gambini, M. Manno, and M. Vellini, 'Numerical analysis and performance assessment of metal hydride-based hydrogen storage systems', *Int. J. Hydrog. Energy*, vol. 33, no. 21, pp. 6178–6187, Nov. 2008.

[23] B. Laoun, 'Thermodynamics aspect of high pressure hydrogen production by water electrolysis', *Revue des Energies Renouvelables*, vol. 10, no. 3, pp. 435–444, 2007.

[24] H. Görgün, 'Dynamic modelling of a proton exchange membrane (PEM) electrolyzer', *Int. J. Hydrog. Energy*, vol. 31, no. 1, pp. 29–38, Jan. 2006.

[25] Hellenic Electricity Distribution Network Operator (HEDNO), 'Monthly Reports of RES & Thermal Units in the non-Interconnected Islands'. [Online]. Available: http://www.deddie.gr/en/themata-tou-diaxeiristi-mi-diasundedemenwn-nisiwn/stoixeia-ekkathariseon-kai-minaion-deltion-mdn/miniaia-deltia-ape-kai-thermikis-paragwgis-sta-mi. [Accessed: 03-Jan-2017].

[26] Ministry of Environment Energy & Climate Change (MEECC), 'National Renewable Energy Action Plan in the Scope of Directive 2009/28/EC'. [Online]. Available: http://www.ypeka.gr/LinkClick.aspx?fileticket=CEYdUkQ719k%3d&tabid=37. [Accessed: 03-Jan-2017].

[27] J. K. Kaldellis, K. Kavadias, and D. Zafirakis, 'The role of hydrogen-based energy storage in the support of large-scale wind energy integration in island grids', *Int. J. Sustain. Energy*, vol. 34, no. 3–4, pp. 188–201, Apr. 2015.

[28] J. K. Kaldellis and D. Zafirakis, 'Optimum energy storage techniques for the improvement of renewable energy sources-based electricity generation economic efficiency', *Energy*, vol. 32, no. 12, pp. 2295–2305, Dec. 2007.

[29] J. K. Kaldellis, K. Kavadias, and J. Garofallakis, 'Renewable energy solution for clean water production in the Aegean Archipelago islands', presented at the Mediterranean Conference on Policies and Strategies for Desalination and Renewable Energies, Santorini, Greece, 2000.

[30] PPC S.A., 'Annual Programme of the Autonomous Power Stations on Non-Inteconnected System', Greece, 2015.

[31] Greek Operator of Electricity Market (LAGIE), 'DAS Monthly Reports-December 2014', 2015.

[32] Department of Energy, 'Fuel Cells', *Office of Energy Efficiency & Renewable Energy*, 2016. [Online]. Available: https://energy.gov/eere/fuelcells/fuel-cells. [Accessed: 13-Jan-2017].

[33] C. Tso, L.-H. Huang, and C.-J. Tseng, 'Hydrogen Scooter Testing and Verification Program', *Energy Procedia*, vol. 29, pp. 633–643, Jan. 2012.